Hindawi
Advances in Civil Engineering
Volume 2021, Article ID 5523668, 13 pages
https://doi.org/10.1155/2021/5523668

Research Article

Stability Assessment of Ground Surface along Tunnels in Karst Terrain Using Improved Fuzzy Comprehensive Evaluation

Kai Zhang[1], **Zelin Zhou**[2,3] **and Shougen Chen**[3]

[1]*College of Civil and Transportation Engineering, Shenzhen University, Shenzhen, Guangdong 518060, China*
[2]*China 19th Metallurgical Corporation, Chengdu, Sichuan 610031, China*
[3]*School of Civil Engineering, Southwest Jiaotong University, Chengdu, Sichuan 610031, China*

Correspondence should be addressed to Zelin Zhou; zhouzelin2021@19mcc.com.cn

Received 17 January 2021; Revised 22 February 2021; Accepted 6 March 2021; Published 18 March 2021

Academic Editor: Xun Xi

The stability of ground surface along tunnels in karst terrain is influenced by complex factors, among which the karst features are the significant ones. Under the influence of karst, the ground surface along tunnels is very easy to collapse, thus causing great casualties and economic losses. To provide guidance for maintaining the stability of ground surface along tunnels, an analysis system is proposed for assessing the stability of ground surface along tunnels in karst terrain based on an improved fuzzy comprehensive evaluation. Based on the case analysis of ground collapse along tunnels in karst terrain and the review of the related researches, the evaluation index system for ground surface stability assessment was established. The ridge-shaped membership functions were constructed to calculate the membership degree for the evaluation indices. The comprehensive weighting method combining the Fuzzy Analytical Hierarchy Process and correlation analysis was applied to determine weights for evaluation indices. And the ground surface stability level was recognized based on the maximum membership principle. The proposed assessment system was applied to assess the ground surface stability along the tunnels of Guiyang Metro Line 1, and the assessment results agreed well with the regional ground collapse history, verifying the effectiveness and reliability of the assessment system. Combining with the assessment results, a series of measures were conducted to promote the ground surface stability before tunnel excavation. This system provides a valuable tool for assessing and guiding to improve stability of the ground surface along tunnels in karst terrain.

1. Introduction

During tunneling in karst terrain, the excavation disturbance can easily cause instability of karst caves and then leads to the ground surface collapse. Because of the complex karst phenomena, the ground collapse in karst terrain has the characteristics of invisibility, burstiness, and mass occurrence [1, 2]. Once the ground collapse happens in the karst terrain, it may cause great casualties and economic losses [3–7]. Recently, more and more efforts have been made in the development and utilization of underground space, and thousands of tunnels have been constructed in karst terrain all over the world, resulting in the fact that hundreds of ground collapses caused by tunnel construction have happed [8–10]. For example, the construction of the Jinshazhou tunnel on the Wuhan-Guangzhou railway led to 19 ground collapses in the Jinshazhou area in Guangzhou, Guangdong Province in the Southern Karst region of China. As a result, the stability of up to 120000 m^2 buildings on the ground was threatened, and more than 260 households were forced to relocate [11]. Another example is that the ground collapse caused by Wuhan metro tunnel excavation in the karst areas resulted in four people falling and died in the collapse pits and millions of RMB of economic losses. In addition, the ground collapse along the tunnel line can also bring problems for tunnel construction. Therefore, assessing the ground surface stability along tunnels is significant for guiding the prevention of ground collapse disaster.

As one of the thorniest problems in the engineering geology field, karst ground surface stability has been given

great emphasis, and numbers of related studies have been conducted. Based on the factors influencing ground surface stability, some mathematical analysis methods, including favorability functions approach [12], curvature analysis [13], geographically weighted regression [14], logistic regression [15, 16], and weights-of-evidence analysis [17], have been applied to assess stability or susceptibility of karst ground. Investigations on the karst phenomenon [18] and geological and hydrogeological conditions [19] were also used to assess the regional karst ground surface stability status. In addition, the numerical simulation methods, including FEM approach [20], DEM approach [21], and physical modeling method [22], have been used to study the stability of karst cavities. However, the researches on ground surface stability related to tunneling in karst terrain are limited. Song et al. [23] and Valenzuela et al. [24] assessed the influence of karst sinkholes on the construction of the Sol-a tunnel in South Korea and Pajares tunnels in Spain, respectively. He et al. [25] assessed the risk of ground collapse along tunnels based on expert judgment.

The existing researches are valuable for studying karst ground surface stability. But for assessing the stability of ground surface along tunnels in karst terrain, there are still limitations. Most of the above-mentioned researches mainly focused on the approaches of data acquisition or data processing but little attention is paid to the recognition of stability degree. Geological and hydrogeological investigation is the most intuitive method for analyzing the stability of karst ground, but the reliability of the results mainly depends on the accuracy of data acquisition. And the investigations cannot be widely used considering the cost and site conditions. As the characteristics of karst are various in different regions, the research results from investigations for karst ground surface stability in specific regions lack universal applicability. Ground surface stability in karst terrain is influenced by complicated factors; the numerical and physical models cannot reflect the real situations of karst geology. And the assessment based on expert judgments was much subjective, making it lacking reliability.

This paper aims to establish an analysis model for assessing the stability of ground surface along tunnels in karst terrain using an improved fuzzy comprehensive evaluation method. The evaluation index system is firstly established based on the analysis of ground collapse cases and review of related researches. The ridged membership functions are applied to calculate the membership degree of evaluation indices. The comprehensive weighting method combining the Fuzzy Analytical Hierarchy Process (FAHP) and correlation analysis is applied to distribute weights for evaluation indices, and the stability level is recognized based on the maximum membership principle. And the proposed assessment system was applied to assess the stability of the ground surface along the tunnel of Guiyang Metro Line 1 to verify its effectiveness and reliability. The proposed assessment system is of great significance for maintaining the stability of ground surface along tunnels in karst terrain.

2. Methodology

The fuzzy comprehensive evaluation is a significant method which can be applied to address the issues with uncertain and fuzzy boundary and has been widely used in fuzzy mathematics [26, 27]. The fuzzy comprehensive evaluation method is improved and applied to establish an assessment system for ground stability in this research and the main work consists of the following parts: establishment of evaluation index system, establishment of index and evaluation sets, membership functions and membership matrix, weights distribution for evaluation indices, and fuzzy comprehensive evaluation matrix [28–30].

2.1. Evaluation Index System. The stability of ground surface along tunnels in karst terrain is affected by complex factors, which can be divided into internal and external factors. The internal influence factors refer to these geological and hydrogeological conditions, while the external factors refer to the engineering ones.

2.1.1. Karst Development Degree. Underground karst is the major factor influencing ground surface stability during tunneling. The percentage of number of boreholes that encountered karst in the total number of boreholes (PBK) is recommended to reflect the density of underground karst [31]. The higher the PBK, the higher the degree of underground karst development. Formation lithology is one of the major factors controlling underground kart development. The formation solubility coefficient (FSC) is defined to describe the solubility of the rock formations. The FSC is calculated by the formula $\mathrm{FSC} = 0.636t_1 + 0.259t_2 + 0.105t_3$, where t_1, t_2, and t_3 are proportions of lithology with strong, medium, and weak solubility, respectively [32], and the formation lithologies with strong, medium, and weak solubility have been defined by Zhang et al. [33]. In general, the higher FSC always contributes to a higher karst development degree.

2.1.2. Bedrock Covering State. The ground surface stability in karst terrain is closely related to the bedrock covering state. The thickness of bedrock covering (TBC) and structural features of bedrock covering (SFBC) are the two major factors seriously influencing ground surface stability. In general, the thinner bedrock covering contributes to a higher probability of ground collapse under specific geological and hydrogeological conditions. The velocity and scale of the ground collapse are highly influenced by the features of bedrock covering, among which the amount and permeability of the layers forming the bedrocks are the two major factors influencing the stability of the bedrock covering.

2.1.3. Groundwater State. The groundwater state, including groundwater hydrodynamic condition (GHC) and distance between groundwater table and bedrock top (DGTB), also strongly influences the stability of ground in karst terrain. The higher content and better runoff conditions of the

groundwater generally contribute to a higher degree of karst development. And the flowing groundwater can also wash away the soil particles and dissolved debris of the karst caves. In addition, fluctuation of groundwater table can change the physical and mechanical properties of surrounding rock or soil of karst caves, resulting in instability of underground cavities, and then induce ground surface stability.

2.1.4. Geological Structure Conditions. The influences of geological structures, including fault and fold, are also other factors influencing the stability of ground in karst terrain. Under the influence of geological structures, numbers of joints and cracks are generated inside the rocks subjected to the in situ stress. The joints and cracks will increase the permeability of the rock and make it susceptible to dissolution and scouring of groundwater, providing favorable conditions for karst development. In addition, the underground caves are extremely unstable in the areas where faults and folds are easy to collapse under the function of external disturbances.

2.1.5. Tunneling Engineering Features. Tunneling engineering features are the external factors influencing the stability of ground surface along the tunnels in karst terrain. Firstly, the excavation of the tunnel can cause a change in the groundwater table. The change of groundwater table can result in a change of buoyancy on the rock mass. The state of force balance state of the karst caves will be broken by the change of buoyancy, easily leading to the collapse of karst caves. The depth of the proposed tunnel also influences ground surface stability. The deeper the tunnel, the more stable the ground above the tunnel, no matter whether there are caves in the ground or not.

Based on cases analysis of ground collapse in karst terrain and review of the related researches [14, 15, 28, 34–39], the following ten factors, PBK, FSC, TBC, SBC, GHC, DGB, width of fault and its influence zone (WFI), structural features of fold (SFF), depth of the proposed tunnel (DPT), and groundwater table change caused by excavation of the proposed tunnel (GCE), were selected to access stability of ground surface along tunnels in karst terrain. A hierarchy structure for assessing the stability of ground surface along tunnels in karst terrain was constructed as presented in Figure 1. And the ten evaluation indices, I_1–I_{10}, were quantitatively graded as shown in Table 1 [11, 17, 25, 30–32, 40, 41].

2.2. Index and Evaluation Sets. Based on the selected evaluation indices, the evaluation index set for assessment of ground surface stability was constructed as follows:

$$\mathbf{I} = \{I_1, I_2, \ldots, I_n\}. \tag{1}$$

As the evaluation indices and the ground surface stability have been divided into four levels as shown in Table 1, the evaluation set was constructed as follows:

$$\mathbf{V} = \{v_1, v_2, \ldots, v_m\}. \tag{2}$$

2.3. Membership Functions and Membership Matrix. There are several membership functions, including triangular, trapezoid, Gaussian, parabolic, and ridged, which can be used to calculate the membership degree for evaluation indices in a fuzzy comprehensive evaluation. Considering the characteristics of the evaluation indices of stability of ground surface along tunnels in karst terrain, the ridged membership function was applied to calculate the membership degrees for evaluation indices in this research [41]. The ridged membership functions consist of smaller, medium, and larger forms, which were presented as equations (3)–(5), respectively:

$$\mu_{i1}(x) = \begin{cases} 1, & x \le a_1, \\ \dfrac{1}{2} - \dfrac{1}{2}\sin\dfrac{\pi}{a_2 - a_1}\left(x - \dfrac{a_1 + a_2}{2}\right), & a_1 < x \le a_2, \\ 0, & x > a_2, \end{cases} \tag{3}$$

$$\mu_{ij}(x) = \begin{cases} 0, & x \le -a_2, \\ \dfrac{1}{2} + \dfrac{1}{2}\sin\dfrac{\pi}{a_2 - a_1}\left(x - \dfrac{a_1 + a_2}{2}\right), & -a_2 < x \le -a_1, \\ 1, & -a_1 < x \le a_1, \\ \dfrac{1}{2} - \dfrac{1}{2}\sin\dfrac{\pi}{a_2 - a_1}\left(x - \dfrac{a_1 + a_2}{2}\right), & a_1 < x \le a_2, \\ 0, & x > a_2, \end{cases} \tag{4}$$

$$\mu_{i4}(x) = \begin{cases} 0, & x \le a_1, \\ \dfrac{1}{2} + \dfrac{1}{2}\sin\dfrac{\pi}{a_2 - a_1}\left(x - \dfrac{a_1 + a_2}{2}\right), & a_1 < x \le a_2, \\ 1, & x > a_2, \end{cases} \tag{5}$$

where $1 \le i \le 10$, $1 \le j \le 4$, $\mu_{ij}(x)$is the membership degree of evaluation index I_i with regard to evaluation level v_j, and a_1 and a_2 are interval thresholds. Figure 2 shows curves of smaller, medium, and larger ridged membership functions, respectively, where t is the critical value of the range corresponding to a stable level for each evaluation index. The interval thresholds a_1 and a_2 are determined using the coefficient amplification method, which was presented as follows:

$$\begin{cases} a_1 = t(1 - \eta), \\ a_2 = t(1 + \eta), \end{cases} \tag{6}$$

where t is the critical value of the index value range and η is the amplification coefficient which is determined according to the related regulations and expert judgments and generally is taken as 0.05–0.3 [42]. In this research, the

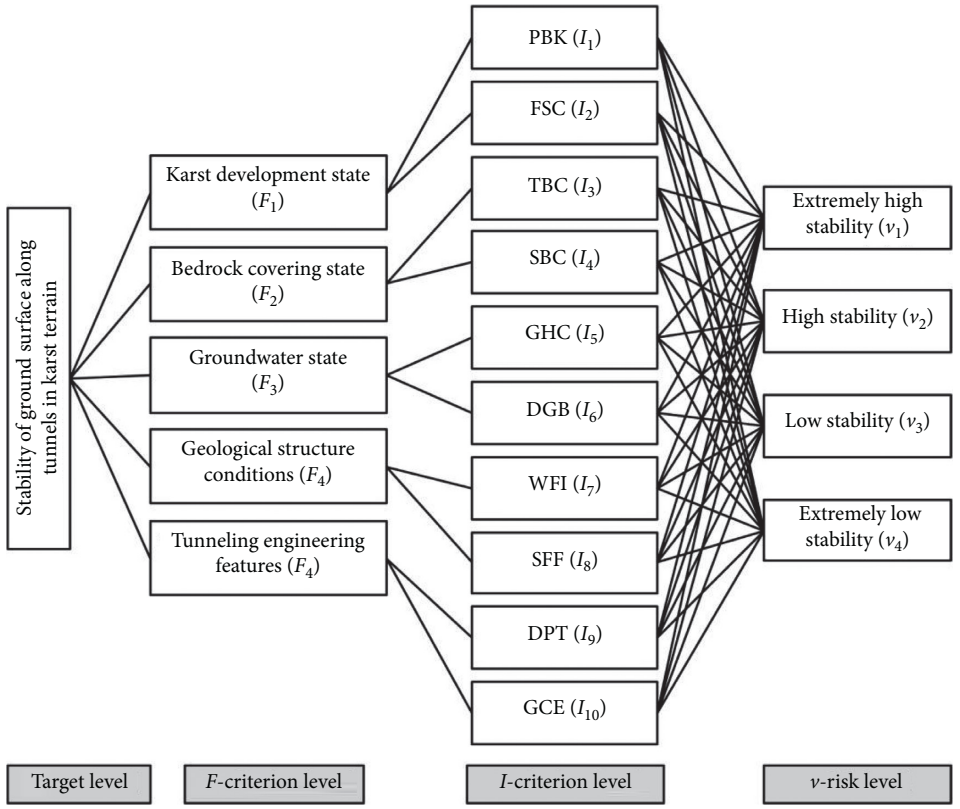

Figure 1: Hierarchy structure for assessing the stability of ground surface along tunnels in karst terrain.

Table 1: Grading standards for evaluation indices.

Evaluation index		Stability level			
		v_1	v_2	v_3	v_4
I_1	PBK (%)	0–10	10–30	30–50	50–100
I_2	FLC	0–0.042	0.042–0.104	0.104–0.254	0.254–0.636
I_3	TBC (m)	20–50	10–20	5–10	0–5
I_4	SBC	0–25 Uniform structure	25–50 Double-layer structure and permeability of the upper layer is lower than that of the lower layer	50–75 Multilayer structure and permeability of the upper layer is lower than that of the lower layer	75–100 Multilayer structure and permeability of the upper layer is higher than that of the lower layer
I_5	GHC	0–25 Groundwater runoff condition is poor	25–50 Groundwater runoff condition is moderate	50–75 Groundwater runoff condition is good	75–100 Groundwater runoff condition is very good
I_6	DGB (m)	10–50	5–10	2.5–5	0–2.5
I_7	WFI (m)	0–3	3–5	5–10	10–50
I_8	SFF	0–25 No fold or the tunneling area locates in the limb parts of flat and open folds	25–50 The tunneling area locates in the limb parts of steep and tight folds	50–75 The tunneling area locates in the hinge parts of flat and open folds	75–100 The tunneling area locates in the hinge parts of steep and tight folds
I_9	DPT (m)	50–100	30–50	10–30	0–10
I_{10}	GCE (m)	0–2	2–5	5–10	10–50

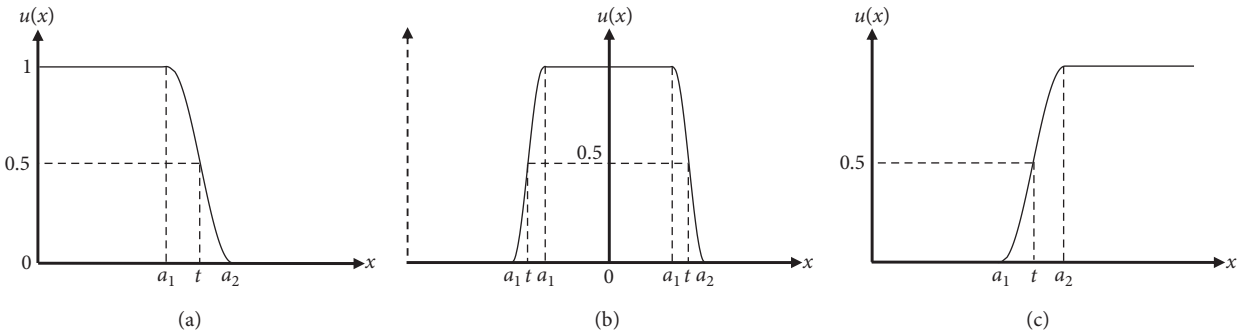

Figure 2: Ridged membership function curves: (a) partial small-scale, (b) middle-scale, and (c) partial large-scale.

proportion for enlarging and reducing was determined as 0.2 based on actual situations and the expert judgments.

Based on the grading standards for evaluation indices shown in Table 1, the membership functions for the ten evaluation indices were constructed and the curves were presented in Figure 3.

When the values of the evaluation indices are obtained, the membership degrees of the evaluation indices can be calculated by substituting the evaluation index values into the above membership functions. Then, a membership matrix can be constructed as follows, where $n = 10$ and $m = 4$ in this research:

$$\mathbf{U} = \begin{bmatrix} u_{11} & \cdots & u_{im} \\ & \ddots & \\ u_{n1} & & u_{nm} \end{bmatrix}. \tag{7}$$

2.4. Weights for Evaluation Indices. The weights for evaluation indices reflect the contribution of the index to the object to be evaluated; the weight matrix of the evaluation indices for ground surface stability is defined as follows:

$$\mathbf{W} = [\mathbf{w}_1, \mathbf{w}_2, \ldots, \mathbf{w}_n], \tag{8}$$

where $\mathbf{w}_i$ is the comprehensive weight of evaluation index I_i, and the weights are assigned through the combination weighting method. The comprehensive weight for the evaluation index consists of subjective and objective weight as shown in equation (14):

$$\begin{aligned} w_i &= w_{io}k_o + w_{is}k_s, \\ k_o + k_s &= 1, \end{aligned} \tag{9}$$

where w_{is} and w_{io} are subjective and objective weights, respectively, and k_s and k_o are proportion coefficients of subjective weight and objective weight, respectively.

2.4.1. Subjective Weight. The subjective weights for evaluation indices are determined based on the FAHP proposed by Chang [43]. In FAHP, the triangular fuzzy number (TFN) in Table 2 is recommended to represent the relative importance scale between objects [30, 44, 45].

Based on the FAHP, the subjective weights of evaluation indices are determined by the following steps. Firstly, the evaluation indices in *F*- and *I*-criterion levels were pairwise compared according to their contributions to their father node, and the comparison matrixes were constructed as shown in Tables 3–4. Then, the consistency ratio (CI) was computed to verify the consistency of the pairwise comparison matrixes [46]. Thirdly, the weights of evaluation indices in each comparison matrix were calculated fowling the FAHP. As the FAHP has been recorded in literature [33, 44, 45], the weight calculation process is omitted in this research and only the calculation results were presented in Tables 3–4. Finally, the global weights for all the evaluation indices were synthesized and presented in Table 5. So, the subjective weight set for evaluation indices was established as follows:

$$\mathbf{w}_s = [\,0.2087,\ 0.1037,\ 0.1099,\ 0.1099,\ 0.0883,\ 0.0883,\ 0.0478,\ 0.0238,\ 0.0730,\ 0.1467\,]. \tag{10}$$

2.4.2. Objective Weights. The objective weights for evaluation indices are determined through correlation analysis of the values of evaluation indices.

Firstly, the evaluation indices should be nondimensionalized to reduce the influence of difference units on the assessment results and make the different indices comparable. In this research, the evaluation index values were linearly nondimensionalized using the following forms:

(a) If the larger values contribute to the higher evaluation levels, take

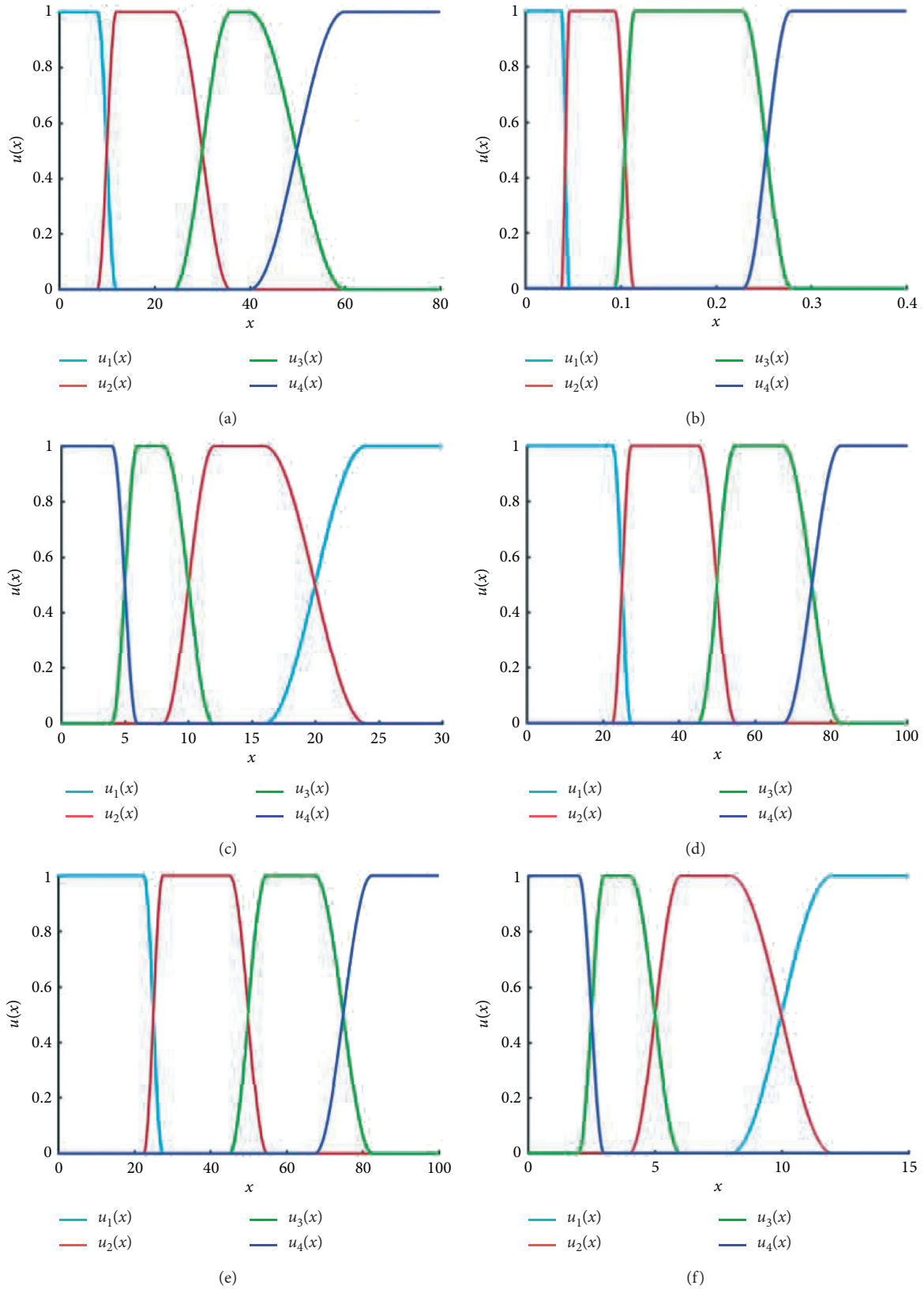

Figure 3: Continued.

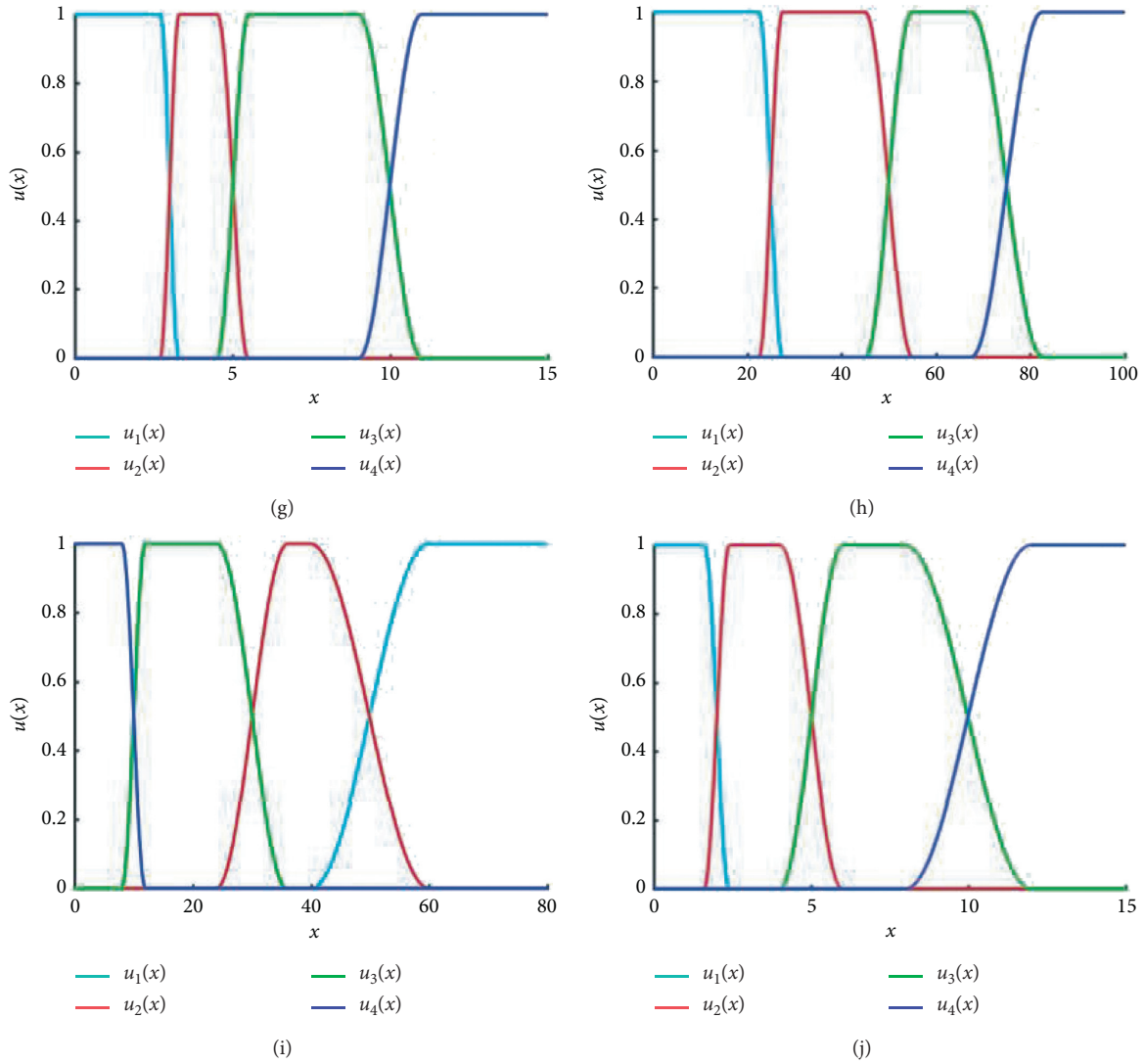

Figure 3: Ridged membership functions for evaluation indices.

Table 2: Explanation of triangular fuzzy number.

Fuzzy number	Explanation	TFN	Inverse TFN
$\tilde{1}$	One object is equally important to the other	(1, 1, 1)	(1, 1, 1)
$\tilde{3}$	One object is slightly important than the other	(1, 3, 5)	(1/5, 1/3, 1)
$\tilde{5}$	One object is moderately important than the other	(3, 5, 7)	(1/7, 1/5, 1/3)
$\tilde{7}$	One object is strongly important than the other	(5, 7, 9)	(1/9, 1/7, 1/5)
$\tilde{9}$	One object is extremely important than the other	(7, 9, 11)	(1/11, 1/9, 1/7)
$\tilde{2}$	Intermediate values between the above two adjacent judgments	(1, 2, 4)	(1/4, 1/2, 1)
$\tilde{4}$		(2, 4, 6)	(1/6, 1/4, 1/2)
$\tilde{6}$		(4, 6, 8)	(1/8, 1/6, 1/4)
$\tilde{8}$		(6, 8, 10)	(1/10, 1/8, 1/6)

Table 3: Weight analysis of indices at F-criterion level.

Evaluation index	F_1	F_2	F_3	F_4	F_5	Weight
F_1	(1, 1, 1)	(1, 3, 5)	(1, 3, 5)	(3, 5, 7)	(1, 3, 5)	0.3124
F_2	(1/5, 1/3, 1)	(1, 1, 1)	(1, 2, 4)	(1, 3, 5)	(1, 1, 1)	0.2197
F_3	(1/5, 1/3, 1)	(1/4, 1/2, 1)	(1, 1, 1)	(1, 3, 5)	(1/4, 1/2, 1)	0.1765
F_4	(1/7, 1/5, 1/3)	(1/5, 1/3, 1)	(1, 3, 5)	(1, 1, 1)	(1/5, 1/3, 1)	0.0716
F_5	(1/5, 1/3, 1)	(1, 1, 1)	(1, 2, 4)	(1, 3, 5)	(1, 1, 1)	0.2197

CI = 0.027 < 0.1, meeting the consistency requirement.

Table 4: Weight analysis of indices I_1–I_{10}.

Evaluation index	I_1	I_2	Weight
I_1	(1, 1, 1)	(1, 2, 4)	0.6679
I_2	(1/4, 1/2, 1)	(1, 1, 1)	0.3321
	I_3	I_4	
I_3	(1, 1, 1)	(1, 1, 1)	0.5000
I_4	(1, 1, 1)	(1, 1, 1)	0.5000
	I_5	I_6	
I_5	(1, 1, 1)	(1, 1, 1)	0.5000
I_6	(1, 1, 1)	(1, 1, 1)	0.5000
	I_7	I_8	
I_7	(1, 1, 1)	(1, 2, 4)	0.6679
I_8	(1/4, 1/2, 1)	(1, 1, 1)	0.3321
	I_9	I_{10}	
I_9	(1, 1, 1)	(1/4, 1/2, 1)	0.3321
I_{10}	(1, 2, 4)	(1, 1, 1)	0.6679

CI = 0 < 0.1, meeting the consistency requirement.

Table 5: Subjective weights for evaluation indices.

Evaluation index	F-level index weight					Subjective weight
	F_1 0.3124	F_2 0.2197	F_3 0.1765	F_4 0.0716	F_5 0.2197	
I_1	0.6679					0.2087
I_2	0.3321					0.1037
I_3		0.5000				0.1099
I_4		0.5000				0.1099
I_5			0.5000			0.0883
I_6			0.5000			0.0883
I_7				0.6679		0.0478
I_8				0.3321		0.0238
I_9					0.3321	0.0730
I_{10}					0.6679	0.1467

$$\begin{cases} \widetilde{x}_i = \dfrac{x_i}{(b_{iP} - a_{iP})}, \\ \widetilde{a}_{ij} = \dfrac{(a_{ij} - a_{iP})}{(b_{iP} - a_{iP})}, \\ \widetilde{b}_{ij} = \dfrac{(b_{ij} - a_{iP})}{(b_{iP} - a_{iP})}. \end{cases} \tag{11}$$

(b) If the larger values contribute to the lower evaluation levels, take

$$\begin{cases} \widetilde{x}_i = \dfrac{x_i}{(a_{iP} - b_{iP})}, \\ \widetilde{a}_{ij} = \dfrac{(a_{iP} - a_{ij})}{(a_{iP} - b_{iP})}, \\ \widetilde{b}_{ij} = \dfrac{(a_{iP} - b_{ij})}{(a_{iP} - b_{iP})}. \end{cases} \tag{12}$$

Here, $\widetilde{x}_i$, $\widetilde{a}_{ij}$, and $\widetilde{b}_{ij}$ are the nondimensionalized values of x_i, a_{ij}, and b_{ij}, $[a_{iP}, b_{iP}]$ is the value range of evaluation indices I_i, and $[a_{ij}, b_{ij}]$ is the value range of indices I_i for the stability level v_j.

Secondly, the correlation degree between index value $\widetilde{x}_i$ and the interval $\widetilde{v}_{ij} = [\widetilde{a}_{ij}, \widetilde{b}_{ij}]$ is defined as follows:

$$K_{ij}\left(\widetilde{x}_i, \widetilde{v}_{ij}\right) = \begin{cases} 2\dfrac{\left(\widetilde{x}_i - \widetilde{a}_{ij}\right)}{\left(\widetilde{b}_{ij} - \widetilde{a}_{ij}\right)}, & \widetilde{x}_i \le \dfrac{\left(\widetilde{a}_{ij} + \widetilde{b}_{ij}\right)}{2}, \\ 2\dfrac{\left(\widetilde{b}_{ij} - \widetilde{x}_i\right)}{\left(\widetilde{b}_{ij} - \widetilde{a}_{ij}\right)}, & \widetilde{x}_i \ge \dfrac{\left(\widetilde{a}_{ij} + \widetilde{b}_{ij}\right)}{2}, \end{cases} \tag{13}$$

and the maximum correlation degree is defined as follows:

$$K_{ij\max}\left(\widetilde{x}_i, \widetilde{v}_{ij_{\max}}\right) = \max_{j=1}^{m}\left\{K_{ij}\left(\widetilde{x}_i, \widetilde{v}_{ij}\right)\right\}, \tag{14}$$

where j meets $1 \le j \le m$.

Thirdly, a coefficient r_i is calculated by the following forms:

(a) If the larger index measure x_i contributes to the higher evaluation level, take

$$r_i = \begin{cases} j_{\max} \times \left(1 + K_{ij_{\max}}\left(\widetilde{x}_i, \widetilde{v}_{ij_{\max}}\right)\right), & K_{ij_{\max}}\left(\widetilde{x}_i, \widetilde{v}_{ij_{\max}}\right) \geq -0.5, \\ j_{\max} \times 0.5, & K_{ij_{\max}}\left(\widetilde{x}_i, \widetilde{v}_{ij_{\max}}\right) < -0.5. \end{cases} \tag{15}$$

(b) If the larger index measure x_i contributes to the lower evaluation level, take

$$r_i = \begin{cases} (m - j_{\max} + 1) \times \left(1 + K_{ij_{\max}}\left(\widetilde{x}_i, \widetilde{v}_{ij_{\max}}\right)\right), & K_{ij_{\max}}\left(\widetilde{x}_i, \widetilde{v}_{ij_{\max}}\right) \geq -0.5, \\ (m - j_{\max} + 1) \times 0.5, & K_{ij_{\max}}\left(\widetilde{x}_i, \widetilde{v}_{ij_{\max}}\right) < -0.5. \end{cases} \tag{16}$$

Finally, the weight of the evaluation index can be obtained according to the following equation:

$$w_{is} = \frac{r_i}{\sum_{i=1}^{n} r_i}. \tag{17}$$

2.5. Fuzzy Comprehensive Evaluation Matrix. Based on the weights and membership degrees of evaluation indices, the comprehensive evaluation matrix for ground surface stability can be constructed as follows:

$$\mathbf{C} = \mathbf{W} \cdot \mathbf{U} = \left[\mathbf{w}_1, \mathbf{w}_2, \ldots, \mathbf{w}_n\right] \cdot \begin{bmatrix} u_{11} & \cdots & u_{im} \\ & \ddots & \\ u_{n1} & & u_{nm} \end{bmatrix}. \tag{18}$$

Then, the level of ground surface stability can be recognized based on the maximum membership degree principle, which is expressed as follows:

$$v_s = \left\{ \frac{c_m}{v_m \longrightarrow \max_{i=1}^{m}\left(c_i\right)} \right\}, \tag{19}$$

where v_s is the evaluation level of the object, c_m is the maximum element in the comprehensive evaluation matrix, and v_m is the corresponding evaluation level in the evaluation set.

3. Case Study

3.1. Engineering Background. The Guiyang Metro Line 1 (GML1) with a total length of 33.90 km belongs to the urban rail transit system of Guiyang, a city locates in the Southwest karst region of China. The sixth working section of GML1 with a length of 2284.8 m (23689.0 m–25973.8 m) is located in the limb parts of the Guiyang syncline, and no fault crosses the tunneling area. The strata in the tunneling area consist of block stones, red clay, argillaceous dolomite, and limestone. The groundwater is mainly recharged by infiltration of surface water and groundwater table is higher than metro tunnel floor. Preliminary surveys indicate that karst features are widely distributed in the tunneling area. The ground surface along the metro line is prone to collapse due to the tunnel excavation. To ensure the safety of metro tunnel construction and protect citizens, roads, and facilities on the ground, it is essential to assess the stability of the ground surface along the metro terrain line before construction.

3.2. Evaluation Indices. Before metro tunnel construction, geological and geophysical surveys were conducted. Based on the survey results, the values of the evaluation indices, I_1– I_{10}, were obtained. According to the change of values of evaluation indices, the tunneling area along the sixth section of GML1 was divided into 32 chainage sections and the values of evaluation indices were presented in Table 6.

$$\mathbf{U} = \begin{bmatrix} 0 & 0.0015 & 0.9985 & 0 \\ 0 & 0.4623 & 0.5377 & 0 \\ 0 & 0 & 0 & 1.0000 \\ 1.0000 & 0 & 0 & 0 \\ 0 & 0.8536 & 0.1464 & 0 \\ 0 & 0 & 0.0245 & 0.9755 \\ 1.0000 & 0 & 0 & 0 \\ 0 & 1.0000 & 0 & 0 \\ 0 & 0 & 0 & 1.0000 \\ 0 & 0.4373 & 0.5627 & 0 \end{bmatrix}. \tag{20}$$

3.3. Extension Assessment Results. Based on the values of evaluation indices, the stability of the ground surface along the metro tunnel line of the sixth section of GML1 was assessed by using the analysis model proposed in this research.

3.3.1. Assessment of Ground Surface Stability at Chainage Section 1. The assessment of ground surface stability at chainage section 1 (chainage 23689.0–23832.5 m) was presented to demonstrate the assessment process. The values of evaluation indices at Section 1 were presented in Table 7.

Firstly, the values in Table 8 were substituted into the membership functions (Figure 2) to calculate the membership degrees for the evaluation indices, based on which

Table 6: Values of the evaluation indices.

Chainage section number	Chainage (m)	Evaluation index									
		PBK (%)	FSC	TBC (m)	SBC	GHC	DGB (m)	WFI (m)	SFF	DPT (m)	GCE (m)
1	23689.0–23832.5	35.7	0.105	2.40	10	45	2.10	0	35	4.60	5.08
2	23832.5–23874.7	35.7	0.105	2.70	85	45	1.40	0	35	4.30	5.08
3	23874.7–23887.8	35.7	0.105	3.40	10	45	0.90	0	35	4.30	5.08
4	23887.8–24108.8	9.5	0.105	5.20	85	45	3.34	0	35	17.10	5.08
5	24108.8–24195.0	9.5	0.105	6.30	85	45	0.18	0	35	18.53	5.08
6	24195.0–24260.0	9.5	0.105	6.30	85	45	2.77	0	35	19.62	5.08
7	24260.0–24288.0	9.5	0.105	7.90	90	45	7.90	0	35	14.96	5.08
8	24288.0–24366.3	9.5	0.105	11.90	85	45	11.9	0	35	14.51	5.08
9	24366.3–24489.3	9.5	0.105	4.80	30	45	8.14	0	35	11.13	5.08
10	24489.3–24544.6	9.5	0.105	2.80	10	45	0.10	0	35	17.37	5.08
11	24544.6–24607.1	9.5	0.105	0.56	15	45	2.44	0	35	16.65	5.08
12	24607.1–24616.6	17.6	0.105	0.56	15	60	2.44	0	35	16.65	5.08
13	24616.6–24631.2	17.6	0.105	7.15	70	60	5.98	0	35	3.32	5.60
14	24631.2–24656.7	17.6	0.105	5.42	80	60	3.12	0	35	3.11	5.60
15	24656.7–24687.0	17.6	0.105	6.74	90	60	1.73	0	35	5.37	5.60
16	24687.0–24721.2	17.6	0.105	1.46	15	60	4.04	0	35	10.04	5.60
17	24721.2–24775.3	17.6	0.105	7.90	20	60	0.50	0	35	15.07	5.60
18	24775.3–24779.6	17.6	0.105	5.73	15	60	3.45	0	20	17.76	4.65
19	24779.6–24840.7	17.4	0.105	9.60	80	60	2.29	0	20	28.04	4.65
20	24840.7–24871.6	17.4	0.105	3.70	15	60	9.72	0	20	27.25	4.65
21	24871.6–24900.0	17.4	0.105	3.34	20	60	3.05	0	20	24.58	4.65
22	24900.0–24939.4	17.4	0.105	2.60	80	60	2.77	0	20	19.98	4.65
23	24939.4–25000.0	17.4	0.105	0.78	20	60	1.64	0	20	10.90	4.65
24	25000.0–25056.4	17.4	0.105	9.20	80	60	4.55	0	20	17.58	4.65
25	25056.4–25100.0	17.4	0.105	8.50	80	60	6.40	0	20	18.55	4.65
26	25100.0–25153.2	17.4	0.105	6.40	80	60	2.66	0	20	21.89	4.65
27	25153.2–25230.5	17.4	0.105	8.00	80	60	3.83	0	20	21.94	4.65
28	25230.5–25285.6	17.4	0.105	7.70	80	60	3.53	0	20	22.21	4.65
29	25285.6–25340.0	17.4	0.105	3.50	85	60	1.26	0	20	20.77	4.65
30	25340.0–25400.0	17.4	0.105	7.00	85	60	2.13	0	20	22.37	4.65
31	25400.0–25467.3	17.4	0.105	7.10	85	60	1.44	0	20	21.95	4.65
32	25467.3–25973.8	17.4	0.105	7.40	85	60	2.08	0	20	20.80	4.65

Table 7: Values of evaluation indices at chainage section 1.

Evaluation index	PBK	FSC	TBC	SBC	GHC	DGB	WFI	SFF	DPT	GCE
Value	0.357	0.165	0.952	0.100	0.450	0.958	0.000	0.350	0.954	0.102

Table 8: Nondimensional values of evaluation indices.

Evaluation index	PBK	FSC	TBC	SBC	GHC	DGB	WFI	SFF	DPT	GCE
Value	0.357	0.165	0.952	0.100	0.450	0.958	0.000	0.350	0.954	0.102

Table 9: Correlation analysis for objective weights of evaluation indices.

Index	K_{ij}				$K_{ij\max}$	$j_{\max}$	r_i	w_{io}
	N_1	N_2	N_3	N_4				
c_1	−5.1400	−0.5700	0.5700	−0.5720	0.5700	3	4.710	0.1153
c_2	−3.0000	−0.0323	0.0133	−0.7801	0.0133	3	3.040	0.0744
c_3	−1.1733	−1.5200	−1.0400	0.9600	0.9600	4	7.840	0.1919
c_4	0.8000	−1.2000	−3.2000	−5.2000	0.8000	1	1.800	0.0441
c_5	−1.6000	0.4000	−0.4000	−2.4000	0.4000	2	2.800	0.0686
c_6	−0.3950	−1.1600	−0.3200	0.3200	0.3200	4	5.280	0.1293
c_7	0.0000	−3.0000	−2.0000	−0.5000	0.0000	1	1.000	0.0245
c_8	−0.8000	0.8000	−1.2000	−3.2000	0.8000	2	3.600	0.0881
c_9	−1.8160	−2.5400	−0.5400	0.9200	0.9200	4	7.680	0.1880
c_{10}	−3.0800	−0.0533	0.0320	−0.2460	0.0320	3	3.096	0.0758

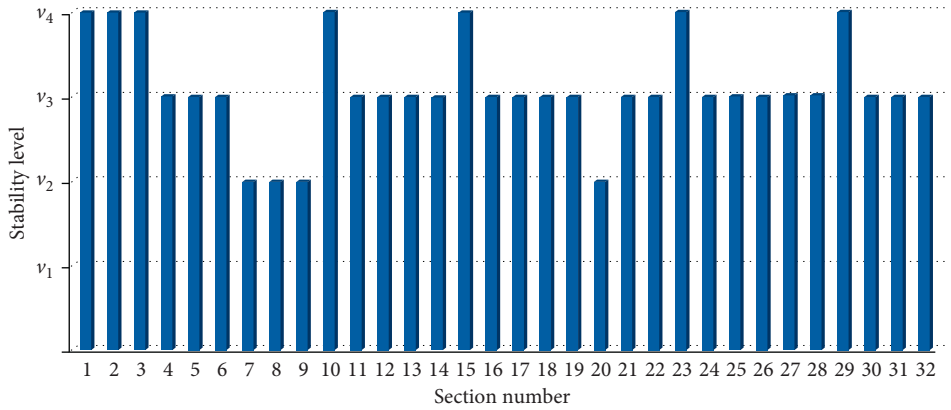

Figure 4: Assessment results of ground surface stability along tunnels in the sixth working section of GML1.

the evaluation matrix was established as shown in equation (20).

Secondly, the objective weights for evaluation indices were determined by using relation analysis. The values of evaluation indices were nondimensionalized according to equations (11) and (12) and the results were presented in Table 8. The objective weights of evaluation indices for chainage section 1 were distributed according to equations (13)–(17) and the results were presented in Table 9.

Combining the subjective weights presented in Table 5, the comprehensive weights of evaluation indices for Section 1 were synthesized according to equation (9), where the proportion coefficients of objective weight and subjective weight are valued as $k_s = k_o = 0.5$ considering the same importance of objective weight and subjective weight for comprehensive weight of evaluation index. So, the weight set was presented as follows:

$$\mathbf{w} = [\,0.1620,\ 0.0891,\ 0.1509,\ 0.0770,\ 0.0784,\ 0.1088,\ 0.0361,\ 0.0560,\ 0.1305,\ 0.1112\,]. \tag{21}$$

Finally, the comprehensive evaluation matrix was established as the following form according to equation (17). And the ground surface stability level was recognized as v_4 according to equation (19).

$$\mathbf{C} = [\,0.1131\ \ 0.2130\ \ 0.2864\ \ 0.3876\,]. \tag{22}$$

3.3.2. Assessment of Ground Surface Stability for the Sixth Working Section of GML1. The stability of ground surface for other chainage sections was assessed in the same way used for stability assessment for chainage section 1, and the assessment results for ground surface stability along tunnels in the sixth working section of GML1 were presented in Figure 4.

3.4. Regional Ground Collapse History. From the stability assessment results, it could be seen that the ground surface stability was medium (N_2) only in chainage sections 7–9 while the stability was low (N_3) or extremely low (N_4) at the rest of chainages. The amount of chainage sections with low or extremely low ground surface stability (28) takes 87.5% of the total section numbers (32). And the length of chainages with low or extremely low ground surface stability (1906.8 m) takes 83.46% of the total length of the sixth working section of GML1 (2284.8 m). The assessment results indicated that the ground surface stability along the metro tunnel was relatively low as a whole.

Correspondingly, the statistics show that more than 50 ground collapses, whose collapse pit diameter (d) is larger than 5 m, caused by human activity had occurred in the urban area of Guiyang city induced by 1998, including about 30 medium-scale collapses ($5\,\text{m} < d < 10\,\text{m}$), 12 large-scale collapses ($10\,\text{m} < d < 20\,\text{m}$), and 8 huge-scale collapses ($d > 20\,\text{m}$). According to the design, the sixth working section of GML1 would pass through the areas where ground collapse had occurred. It indicated that the ground collapse was prone to occur during the excavation of the metro tunnel. So, the assessment results of ground surface stability agreed well with the history of ground collapse at the sixth working section of GML1, which confirmed the effective and reasonable effectiveness and rationality of the fuzzy comprehensive evaluation system for ground surface stability proposed in this research.

3.5. Engineering Countermeasures. Based on the assessment results of ground surface stability, a series of measures were taken to maintain the stability of the ground surface during the construction of the tunnel of GML1:

(1) The displacement of the ground surface along the entire metro tunnel line was closely monitored, and the ground-penetrating radar was applied to preliminarily detect the underground caves.

(2) Grouting was conducted on the ground in the areas with low or extremely low stability. The grouting

borehole diameters were 159 mm and distances were 2.5 m. The grouting slurry consisted of cement slurry and water glass and their volume ratio was 1 : 0.6.

(3) Grouting on the tunnel face was conducted in the areas where the ground surface stability was extremely low. The grouting holes had a diameter of 10 cm and spacing of 30 to 60 cm. The grouting slurry was composed of cement slurry and water glass, and their volume ratio was 1 : 0.6.

4. Conclusion

This study has established an evaluation system for assessing the stability of ground surface along tunnels in karst terrain using a fuzzy comprehensive evaluation method. The major conclusions were drawn as follows.

The works of stability assessment of ground surface along the tunnel in karst terrain mainly contain establishment of evaluation index system, establishment of membership functions for evaluation indices, weights distribution for evaluation indices, and fuzzy comprehensive evaluation of ground surface stability. The selection and quantitatively grading for evaluation indices were conducted based on related case analysis and review of related researches. The evaluation index weights were determined by a comprehensive weighting method combining the FAHP and correlation analysis. These characteristics make the proposed evaluation system a reliable tool for assessing the stability of ground surface along tunnels in karst terrain.

The comprehensive weighting method was applied to distribute weights for evaluation indices. The evaluation indices were nondimensionalized during the determination of objective weights for evaluation indices. The nondimensionalization can eliminate the differences of evaluation indices units and make these indices comparable. The comprehensive weighting method combining FAHP and correlation analysis considers not only human subjective cognition but also factual information of objects, which can highly reduce the errors generated by using a single weighting method and significantly improve the accuracy of evaluation indices weights.

The proposed fuzzy comprehensive evaluation system was applied to assess the stability of the ground surface along the metro tunnel of the sixth working section of GML1. The assessment results agreed well with the history of regional ground collapse, indicating that the assessment results were reliable. The proposed evaluation system provides a valuable tool for assessing and guiding to improve stability of ground along tunnels in karst terrain, and the methodology proposed in this research can be also referred to solve other decision-making problems in engineering, such as water inrush risk, slope stability analysis, and method selection for tunnel construction.

The proposed evaluation system inevitably has limitations. Some of the evaluation indices are quantitatively graded with certain subjective. As the membership functions are closely related to grading standards of the evaluation indices, the evaluation index system highly affects the assessment result, which should be improved in the future research.

Data Availability

The data included in this study are available from the corresponding author upon request.

Conflicts of Interest

The authors declare that they have no conflicts of interest.

Acknowledgments

This work was supported by the National Natural Science Foundation of China (no. 52004163) and the China Postdoctoral Science Foundation (no. 2020M682892).

References

[1] F. Gutiérrez, M. Parise, J. De Waele, and H. Jourde, "A review on natural and human-induced geohazards and impacts in karst," *Earth-Science Reviews*, vol. 138, pp. 61–88, 2014.

[2] X. Xi, Z. Yin, S. Yang, and C. Li, "Using artificial neural network to predict the fracture properties of the interfacial transition zone of concrete at the meso-scale," *Engineering Fracture Mechanics*, vol. 242, Article ID 107488, 2021.

[3] Ó Pueyo Anchuela, A. M. Casas Sainz, A. Pocoví Juan, and H. Gil Garbí, "Assessing karst hazards in urbanized areas. Case study and methodological considerations in the mantle karst from Zaragoza city (NE Spain)," *Engineering Geology*, vol. 184, pp. 29–42, 2015.

[4] M. Parise, D. Closson, F. Gutiérrez, and Z. Stevanović, "Anticipating and managing engineering problems in the complex karst environment," *Environmental Earth Sciences*, vol. 74, no. 12, pp. 7823–7835, 2015.

[5] X. Xi, X. Wu, Q. Guo, and M. Cai, "Experimental investigation and numerical simulation on the crack initiation and propagation of rock with pre-existing cracks," *IEEE Access*, vol. 8, pp. 129636–129644, 2020.

[6] T. Zhang, M. Pang, X. Zhang, and H. Pan, "Determining the seepage stability of fractured coal rock in the karst collapse pillar," *Advances in Civil Engineering*, vol. 2020, no. 8, 11 pages, Article ID 1909564, 2020.

[7] B. Yu, Z. Chen, and J. Wu, "Experimental investigation on seepage stability of filling material of karst collapse pillar in mining engineering," *Advances in Civil Engineering*, vol. 2018, no. 8, 10 pages, Article ID 3986490, 2018.

[8] Z. Chu, Z. Wu, Q. Liu, and B. Liu, "Analytical solution for lined circular tunnels in deep viscoelastic Burgers rock considering the longitudinal discontinuous excavation and sequential installation of liners," *Journal of Engineering Mechanics (ASCE)*, vol. 147, no. 4, pp. 1–22, 2021.

[9] T. Zhou, J. B. Zhu, Y. Ju, and H. P. Xie, "Volumetric fracturing behavior of 3D printed artificial rocks containing single and double 3D internal flaws under static uniaxial compression," *Engineering Fracture Mechanics*, vol. 205, pp. 190–204, 2019.

[10] H. Xie, J. Zhu, T. Zhou, K. Zhang, and C. Zhou, "Conceptualization and preliminary study of engineering disturbed rock dynamics," *Geomechanics and Geophysics for Geo-Energy and Geo-Resources*, vol. 6, no. 34, pp. 1–14, 2020.

[11] S. Zhou, *Risk Analysis of Karst Collapse in Guangzhou Baiyun District Based on Analytical Hierarchy Process Combined with Probability Calculation*, South China University of Technology, Guangzhou, China, 2012.

[12] J. P. Galve, F. Gutiérrez, P. Lucha et al., "Probabilistic sinkhole modelling for hazard assessment," *Earth Surface Processes and Landforms*, vol. 34, no. 3, pp. 437–452, 2008.

[13] F. Stecchi, M. Antonellini, and G. Gabbianelli, "Curvature analysis as a tool for subsidence-related risk zones identification in the city of Tuzla (BiH)," *Geomorphology*, vol. 107, no. 3-4, pp. 316–325, 2009.

[14] D. H. Doctor and K. Z. Doctor, "Spatial analysis of geologic and hydrologic features relating to sinkhole occurrence in Jefferson county, West Virginia," *Carbonates and Evaporites*, vol. 27, no. 2, pp. 143–152, 2012.

[15] K. Papadopoulou-Vrynioti, G. D. Bathrellos, H. D. Skilodimou, G. Kaviris, and K. Makropoulos, "Karst collapse susceptibility mapping considering peak ground acceleration in a rapidly growing urban area," *Engineering Geology*, vol. 158, pp. 77–88, 2013.

[16] A. Ozdemir, "Sinkhole susceptibility mapping using logistic regression in Karapınar (Konya, Turkey)," *Bulletin of Engineering Geology and the Environment*, vol. 75, no. 2, pp. 681–707, 2016.

[17] J. Perrin, C. Cartannaz, G. Noury, and E. Vanoudheusden, "A multicriteria approach to karst subsidence hazard mapping supported by weights-of-evidence analysis," *Engineering Geology*, vol. 197, pp. 296–305, 2015.

[18] G. Kaufmann and Y. Quinif, "Geohazard map of cover-collapse sinkholes in the "Tournaisis" area, southern Belgium," *Engineering Geology*, vol. 69, no. 4, pp. 523–532, 2002.

[19] J. P. Galve, C. Castañeda, F. Gutiérrez, and G. Herrera, "Assessing sinkhole activity in the Ebro Valley mantled evaporite karst using advanced DInSAR," *Geomorphology*, vol. 229, pp. 30–44, 2015.

[20] M. Z. Yang and E. C. Drumm, "Stability evaluation for the siting of municipal landfills in karst," *Engineering Geology*, vol. 65, no. 2-3, pp. 185–195, 2002.

[21] A. A. Baryakh, S. B. Stazhevskii, E. A. Timofeev, and G. N. Khan, "Strain state of a rock mass above karst cavities," *Journal of Mining Science*, vol. 44, no. 6, pp. 531–538, 2008.

[22] D. J. Goodings and W. Abdullah, "Stability charts for predicting sinkholes in weakly cemented sand over karst limestone," *Engineering Geology*, vol. 65, no. 2-3, pp. 179–184, 2002.

[23] K.-I. Song, G.-C. Cho, and S.-B. Chang, "Identification, remediation, and analysis of karst sinkholes in the longest railroad tunnel in South Korea," *Engineering Geology*, vol. 135-136, pp. 92–105, 2012.

[24] P. Valenzuela, M. J. Domínguez-Cuesta, M. Meléndez-Asensio, M. Jiménez-Sánchez, and J. A. S. de Santa María, "Active sinkholes: a geomorphological impact of the Pajares tunnels (cantabrian range, NW Spain)," *Engineering Geology*, vol. 196, pp. 158–170, 2015.

[25] Z. He, Y. Wei, and J. Huang, "Stability assessment for karst collapse along Xuzhou metro using a comprehensive fuzzy model," *The Chinese Journal of Geological Hazard and Control*, vol. 28, no. 3, pp. 66–72, 2017.

[26] Q. Yao, X. Yang, and H. Li, "A fuzzy AHP-based method for comprehensive blasting vibration comfort evaluation forecast," *Advances in Civil Engineering*, vol. 2020, no. 9, 11 pages, Article ID 8919314, 2020.

[27] Y. Liu, X. Huang, J. Duan, and H. Zhang, "The assessment of traffic accident risk based on grey relational analysis and fuzzy comprehensive evaluation method," *Natural Hazards*, vol. 88, no. 3, pp. 1409–1422, 2017.

[28] Y. Wang, W. Yang, M. Li, and X. Liu, "Risk assessment of floor water inrush in coal mines based on secondary fuzzy comprehensive evaluation," *International Journal of Rock Mechanics and Mining Sciences*, vol. 52, pp. 50–55, 2012.

[29] L. Li, T. Lei, S. Li et al., "Risk assessment of water inrush in karst tunnels and software development," *Arabian Journal of Geosciences*, vol. 8, no. 4, pp. 1843–1854, 2015.

[30] K. Zhang, D. D. Tannant, W. Zheng, S. Chen, and X. Tan, "Prediction of karst for tunnelling using fuzzy assessment combined with geological investigations," *Tunnelling and Underground Space Technology*, vol. 80, pp. 64–77, 2018.

[31] Ministry of Housing and Urban-Rural Development, *Code for Design of Building Foundation*, Ministry of Housing and Urban-Rural Development, Beijing, China, 2012.

[32] S.-c. Li, Z.-q. Zhou, L.-p. Li, Z.-h. Xu, Q.-q. Zhang, and S.-s. Shi, "Risk assessment of water inrush in karst tunnels based on attribute synthetic evaluation system," *Tunnelling and Underground Space Technology*, vol. 38, pp. 50–58, 2013.

[33] K. Zhang, W. Zheng, C. Xu, and S. Chen, "An improved extension system for assessing risk of water inrush in tunnels in carbonate karst terrain," *KSCE Journal of Civil Engineering*, vol. 23, no. 5, pp. 2049–2064, 2019.

[34] A. R. Farrant and A. H. Cooper, "Karst geohazards in the UK: the use of digital data for hazard management," *Quarterly Journal of Engineering Geology and Hydrogeology*, vol. 41, no. 3, pp. 339–356, 2008.

[35] A. S. d. Santolo, G. Forte, M. De Falco, and A. Santo, "Sinkhole risk assessment in the metropolitan area of Napoli, Italy," *Procedia Engineering*, vol. 158, pp. 458–463, 2016.

[36] A. Santo, P. Budetta, G. Forte, E. Marino, A. Pignalosa, and A. Pignalosa, "Karst collapse susceptibility assessment: a case study on the Amalfi Coast (Southern Italy)," *Geomorphology*, vol. 285, pp. 247–259, 2017.

[37] H.-J. Oh and S. Lee, "Assessment of ground subsidence using GIS and the weights-of-evidence model," *Engineering Geology*, vol. 115, no. 1-2, pp. 36–48, 2010.

[38] F. Huang, D. Wang, Y. Feng, and M. Zhang, "Prediction of the collapse region induced by a concealed karst cave above a deep highway tunnel," *Advances in Civil Engineering*, vol. 2020, no. 1, 14 pages, Article ID 8825262, 2020.

[39] C. Jiang, H.-s. Xie, J.-l. He, W.-y. Wu, and Z.-c. Zhang, "Analytical solution of seepage field in karst tunnel," *Advances in Civil Engineering*, vol. 2018, no. 1, 9 pages, Article ID 9215472, 2018.

[40] J. Pan, S. Zhou, P. Lin, and Y. Ma, "Preliminary study of risks of karst collapse in Guangzhou Baiyun district," *Rock and Soil Mechanics*, vol. 34, no. 9, pp. 2589–2600, 2013.

[41] K. Zhang, *Study on the Influence of Hidden Karst on the Safety of Tunnel Construction by Mining Method*, Southwest Jiaotong University, Chengdu, China, 2019.

[42] Z. Cui, *Research on the Reliability and Durability of Reinforced Concrete Structure Based on Fuzzy Mathematics*, Jilin Jianzhu University, Changchun, China, 2018.

[43] D.-Y. Chang, "Applications of the extent analysis method on fuzzy AHP," *European Journal of Operational Research*, vol. 95, no. 3, pp. 649–655, 1996.

[44] H. Nezarat, F. Sereshki, and M. Ataei, "Ranking of geological risks in mechanized tunneling by using Fuzzy Analytical Hierarchy Process (FAHP)," *Tunnelling and Underground Space Technology*, vol. 50, pp. 358–364, 2015.

[45] Z. Lu, L. Wu, X. Zhuang, and T. Rabczuk, "Quantitative assessment of engineering geological suitability for multilayer Urban Underground Space," *Tunnelling and Underground Space Technology*, vol. 59, pp. 65–76, 2016.

[46] T. L. Saaty, "Applications of analytical hierarchies," *Mathematics and Computers in Simulation*, vol. 21, no. 1, pp. 1–20, 1979.